Industry Nexus, Volume 1, Issue 1 (2025), 51-60

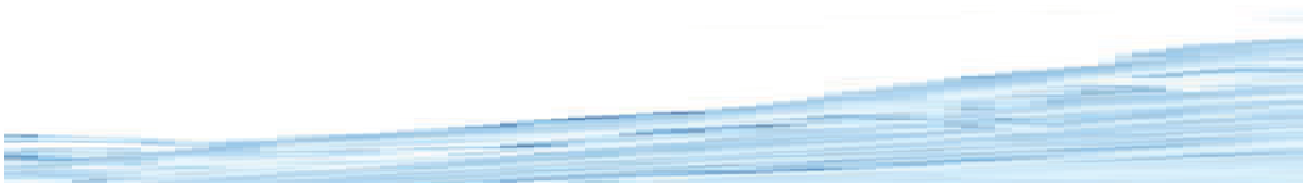

Transient diffusion analysis in a two-dimensional porous domain with varying mass transfer coefficients using comsol multiphysics

Sekar M [1]

[1] Division of Engineering, New York University Abu Dhabi, United Arab Emirates.

(Received 03 January 2025; revised 22 February 2025; accepted 15 March 2025)

Abstract

In the current study the transient diffusion behavior in a two-dimensional porous domain with varying mass transfer coefficients using COMSOL Multiphysics 6.1 was examined. The mass transfer diffusivity was varied from 5 m/s to 10 m/s in the interval of 2.5 m/s. A series of simulation carried out with various mass transfer coefficient in the timesteps size varied between 0 ms to 100 ms. A computational model was developed using COMSOL Multiphysics to simulate the transport phenomenon, governed by the mass conservation equation and appropriate boundary conditions. The left boundary was set as a constant concentration source, while the right boundary employed a Robin condition. The transient concentration distributions, average flux, and total flux streamlines were analyzed for different mass transfer coefficients. The results revealed that higher K values lead to increased concentration gradients and faster diffusion front propagation. In addition to above the raise in the K also plays an crucial role in the rapid boundary concentration depletion, higher peak fluxes, and earlier occurrence of peak flux. However, there is no massive improvement either in the concentration and average flux were noted across wide range of time dependent analysis when the mass transfer coefficient is varied. Nevertheless, for a precise porous dilution application it is mandate to understand the flow of total flux. Thus, the current study provides the limelight to understand the impact of accurately modeling mass transfer boundary conditions on species transport rates in porous domains.

Keywords: Separation process; Catalytic reactions; Species transport; CFD; Mass transfer coefficient.

Email address for correspondence: ms15087@nyu.edu

1.**Introduction**

Engineering and scientific researchers are focusing on species transport in porous media [1]. This process involves controlling the motion of the particles, fluids, and organic matter with the help of porous materials. This method employs materials like soil, rock, and synthetic structures [2]. In environmental engineering, this method helps prevent contamination of groundwater [3]. Industry waste like harmful chemicals and poisonous water can move through the soil like porous media, so researchers can understand the movement of chemicals and avoid contamination of groundwater and agriculture land. In the biochemical field, this process is used to deliver the drugs to a particular location of the human body [4]. Because drug use, like cancer, will affect the rest of the organs as well, this porous media transport helps with drug delivery in the exact location of the affected area. which results in increased safety and better treatment. In chemical engineering, porous media play a vital role in the design of catalysts [5]. This catalyst is made of porous material to increase the efficiency of chemical reactions.

The modelling diffusion of heterogeneous porous media is complex due to its material, size, shape, and connection [6]. Here, heterogeneous media are constructed in an irregular pattern, so the movement of the molecules is not uniform. The pathways of pores are large in some places and very small in others. So this variation will play a major role in modelling porous media. and due to the non-uniform size and shape of the pores, it is difficult to analyse the movement of substances in the medium. The impact of transport properties changes throughout the design due to the non-uniform shape and size of the material [7]. In the conventional method, it considers uniform properties for all mediums, but with this approach, it is not possible to develop an efficient medium. While analyzing the structural heterogeneity of design, an advanced mathematical model and computation facilities are required [8]. A simple model assumes uniformity throughout the system, which will lead to failure. While creating an accurate mathematical model, it needs specific information about the structure, which is not possible to obtain [9]. The collection of accurate data on heterogeneous media structures is challenging. Approaches like imaging and tomography will provide good results but are not accurate [10]. Without accurate results, it is not possible to create accurate models.

The mass transfer coefficient will play a major role in species transport flow rate prediction [11]. This coefficient value determines how fast substances move from one region to another. a high value of the mass transfer coefficient, which will give a faster diffusion rate. The variation of the mass transfer coefficient will influence the species transport rate [12]. The concentration of gradients that develop in the porous medium depends on the mass transfer coefficient. Higher values of coefficient level provide flatter gradients due to their faster surface movement. Lower values of the coefficient create steeper gradients.

The computational model is used in the transient diffusion process. COSMOL and Multiphysics are mainly used in complex geometry and transport for flexibility and faster operation [13]. The diffusion process changes over time, which will be determined by the computational model and provide details of substance movement in the medium. This model solves the equations and provides the concentration profile and dynamics of the system [14]. With the help of a computational model, real-world practical applications of geometrical shapes are solved, and an exact simulation of diffusion is obtained. In the case of analytical methods, it is complex to compute. The properties, such as diffusivity, are not constant, and they will change across the medium. This will be done by the computational model and provide solutions for real-time applications. Applications like COSMOL will provide the flexibility of customization and, with the help of this, fix the boundary conditions and material properties and test the various scenarios [15]. With the help of computational models, the concentration of profiles can be generated in the form of graphs and animations. Simulations of the computational model provide a cost-effective approach instead of real-time experiments [16]. It allows researchers to test different scenarios without a physical setup. So computational models play a major role in studying the diffusion process.

Previous studies on species transport in porous media concentrated on fluids and substance movement in the material, like rock and soil. Which helps in predicting the contamination of soil and water. Some research is focused on the chemical reaction between the porous medium and the solution, which will affect the porous transport. Other studies show how microbial reactions happen inside the media and influence the transport process [17]. In spite of the advancement of porous studies previously done, some notable gaps are also there regarding heterogeneous media, mass coefficients, and scale effects. The objectives of the present study focus on the impact of mass transfer coefficients and how the various coefficient values affect concentration over the time period. To test the heterogeneous porous media with various mass transfer states. and check the average flux of species developed in the medium and how it affects the mass transfer coefficient.

2. Methodology and Modeling

A two-dimensional model was developed in COMSOL Multiphysics 6.1 to simulate the transport of a dilute chemical species through a porous square domain with circular voids [18]. The geometry consists of a 0.8 mm x 0.8 mm square containing an 8x9 array of circles, each with a diameter of 0.06 mm and spaced 0.1 mm apart. The Chemical Species Transport interface was used to model the transient diffusion and convection of the dilute species through the porous domain [19]. The governing equations solved were the mass conservation equation for the species concentration c given by 1,

$$\partial c/\partial t + \nabla\cdot(-D\nabla c) + u\cdot\nabla c = R$$

where D is the diffusion coefficient (m^2/s), u is the velocity vector (m/s), and R is a reaction rate expression for the species ($mol/(m^3s)$).

The following boundary conditions were applied, No Flux to all exterior boundaries of the domain, to represent no species transfer across those boundaries [20]. Left boundary set to a constant concentration of c_{max} = 3 mol/m^3 to act as a continuous source. At the Right boundary set to Outward Flux with a mass transfer coefficient kf = 10 m/s and 0 mol/m^3 external concentration, to allow species outflow

Key input parameters to the model were:

- Diffusion coefficient D2 = 1e-5 m^2/s in the porous domain
- Diffusion coefficient D1 = 2.15e-6 m^2/s in the circular voids (to simulate slower diffusion)
- Initial concentration c0 = c_{max}*exp(a * (-(x/0.4mm)^2)) with peak concentration c_{max}=3mol/m^3 and decay constant a=1000 to provide a non-uniform initial distribution highest near the left boundary
- Porosity epsilon = 0.4002 as a material property

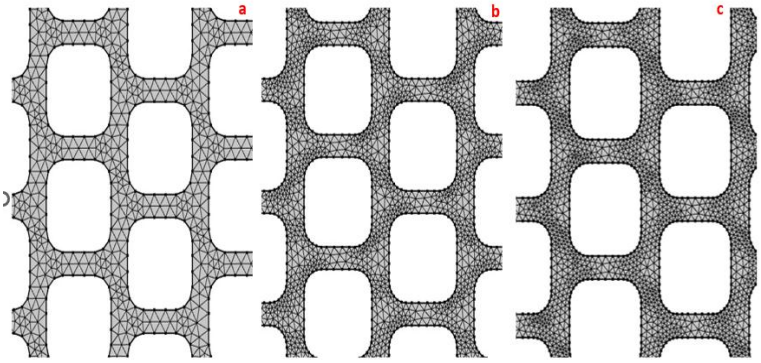

Figure 1. Mesh details a) coarse b) fine c) extra fine

The domain was discretized using a Free Triangular mesh with size coarser, fine and very fine resulting in 5780, 8730, and 12456 domain elements and 532, 1059, and 3456 boundary elements. Figure 1 shows the mesh comparison between all the models. The time-dependent study was solved from 0 to 100 ms with a maximum time step of 2 ms. A Fully Coupled solver using the PARDISO direct solver was selected with a Relative Tolerance of 0.005. Derived values, tables and plots were set up to post-process the results. Average species flux was evaluated on the right boundary using a Boundary Average. A surface plot was generated to visualize the 2D concentration field over time. 1D point graphs plotted both the concentration on the left and right boundaries as well as the average outflow flux on the right boundary vs. time. Data was also tabulated for the average flux and concentrations.

3. Results and discussion

3.1 Transient concentration distributions for diffusion models with varying mass transfer coefficients.

The transient concentration distributions for diffusion models with varying mass transfer coefficients K (2.5 m/s, 5 m/s, 7.5 m/s, 10 m/s) illuminate the spatiotemporal evolution of species concentration over a 50 ms simulation period. These models address the two-dimensional transient diffusion equation ($\partial c/\partial t = \nabla\cdot(D\nabla c)$) [21] subject to the initial condition c0(x,y) = cmax*exp(-a(x/L)²), where cmax=3 mol/m^3, a =1000, and L=0.4 mm, representing a Gaussian distribution peaking near the left boundary (x = 0). Boundary conditions significantly influence the concentration evolution. The left boundary (x = 0) employs a Dirichlet condition with c = cmax, maintaining a constant source. The right boundary (x = L) features a Robin condition, $-D\partial c/\partial x = K(c - cext)$, where D is the diffusion coefficient, K is the mass transfer coefficient, and cext = 0 is the external concentration. This boundary condition represents a mass transfer resistance inversely proportional to K, where increasing K decreases resistance, facilitating faster concentration depletion at the boundary.

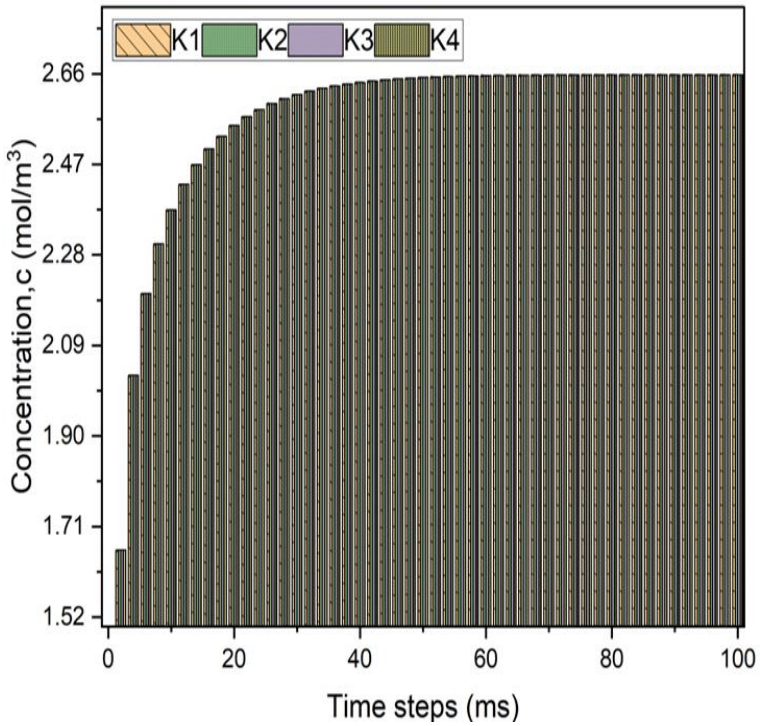

Figure 2. Concertation for various model across different timesteps

Figure 2 shows the effects of the concentration on various timestep of different models. The effect of K on concentration profiles is evident in surface plots. Lower K values (K_1, K_2) yield smaller concentration gradients ($\partial c/\partial x$), indicating slower diffusion. The concentration front, marked by the steepest gradient region, progresses more slowly into the domain. On the contrary, higher values notes for K_3 and K_4 due to larger gradients and more rapid diffusion front advancement. The diffusive flux, $J=-D\nabla c$, quantitatively demonstrates that larger gradients increase flux magnitude.

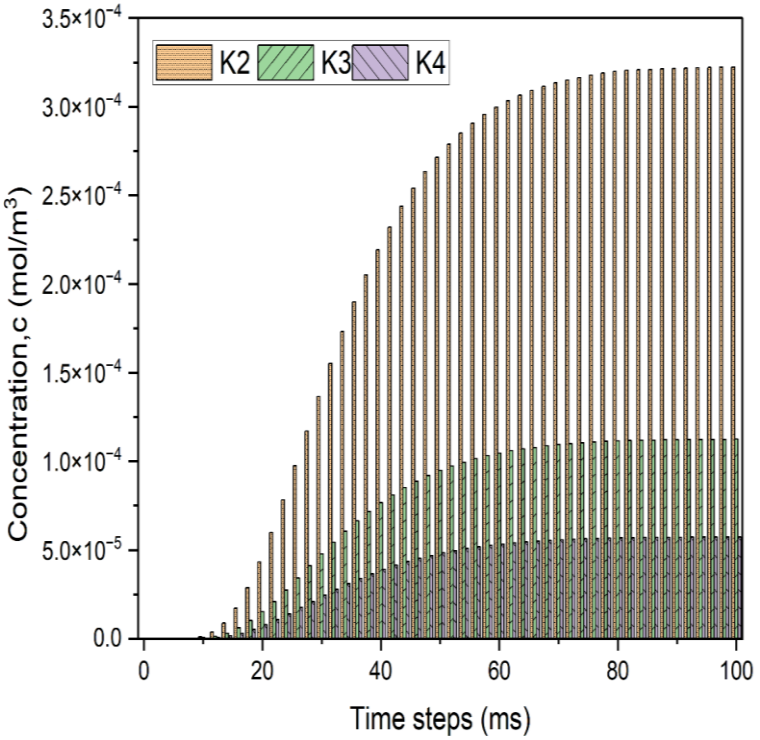

Figure 3. Difference in the Concentration case for K2, k3 and K4 models compared to K1.

Differences in diffusion rates produce distinct concentration distributions over time. Figure 3 represents the difference in the Concentration case for K2, K3 and K4 models compared to K1. By t = 50 ms, models with K3 and K4 exhibit more uniform concentrations, as higher mass transfer rates at the right boundary expedite equilibration. The impact of K is quantified by comparing each model's concentration to the K1. The difference $cKi(t) - cK_1(t)$ grows almost linearly over time, with the K4 model showing the largest nonconformity, followed by K3 and K2. At the timestep of t = 100 ms, these differences reach approximately 2.66 mol/m³, 2.47 mol/m³, and 2.28 mol/m³, respectively.

One-dimensional concentration plots at the boundaries provide further numerical insights and also empathize the difference between each case. At x = 0, concentration remains at cmax due to the Dirichlet condition. At x = L, concentration c(L,t) decays more rapidly and to lower values with increasing K. The analytical solution for c(L,t), derived using Laplace transforms and the semi-infinite medium approximation, is $c(L,t) \approx c_{max} * \text{erfc}(L/\sqrt{4Dt}) * \exp(-KL/D)$, where erfc is the complementary error function. This expression shows explicit dependence on K, with larger K resulting in faster exponential decay.

3.2 Discussion of Average Flux

Average flux results provides insights into species transport rates across the right boundary, governed by the mass transfer boundary condition $-D\partial c/\partial x = K(c - c_{ext})$. The flux J, representing species transport per unit area per unit time, is driven by the concentration gradient per Fick's law, $J = -D\nabla c$ [2].

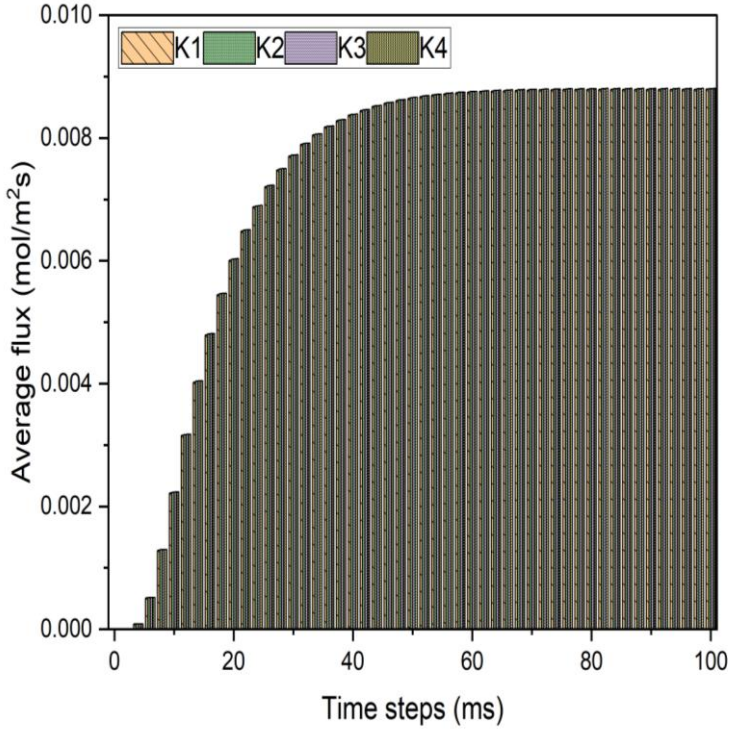

Figure 4. Average flux for various model across different timesteps

Figure 4 shows the average flux for various model across different timesteps. One-dimensional plots of average flux versus time reveal the dynamic behavior of diffusive transport. Initially, flux is zero since the concentration front has not reached the boundary. As the front arrives, flux rapidly increases due to the steep concentration gradient. As gradient is most distinct, then decaying as the concentration field becomes more uniform. Results reveal that K significantly affects flux behavior irrespective of the cases. Higher K values yield higher peak fluxes. A larger K reduces boundary mass transfer resistance, enabling rapid species removal and steeper concentration gradients. The peak flux for the K4 model (K = 10 m/s) nearly doubles that of the K1 model, which eventually shows the substantial impact on maximum transport rate.

The peak flux occurrence time is also influenced by K, with higher K values resulting in early peaks. The analytical solution for flux at the right boundary, J(L,t), obtained by differentiating the concentration solution, is $J(L,t) \approx -D * c_{max} / \sqrt{(\pi Dt)} * \exp(-L^2/(4Dt)) * (1+ KL/D)$. The above expression indicates flux dependence on both D and K, with larger K shifting peak flux to earlier times.

The decay from peak flux to steady state is more rapid for higher K, as evidenced by steeper declines in flux curves. At long timestep size, flux approaches a steady-state value Jss = -D * (cmax - cext) / (L + D/K), dependent on both D and K. Larger K results in marginal increase in the higher steady-state fluxes due to a long-time concentration gradient. Compelling all together, it is evident that K relative impact on steady-state flux is less noticeable than on transient behavior. Figure 5 reports the difference in the average flux case for K2, k3 and K4 models compared to K1.

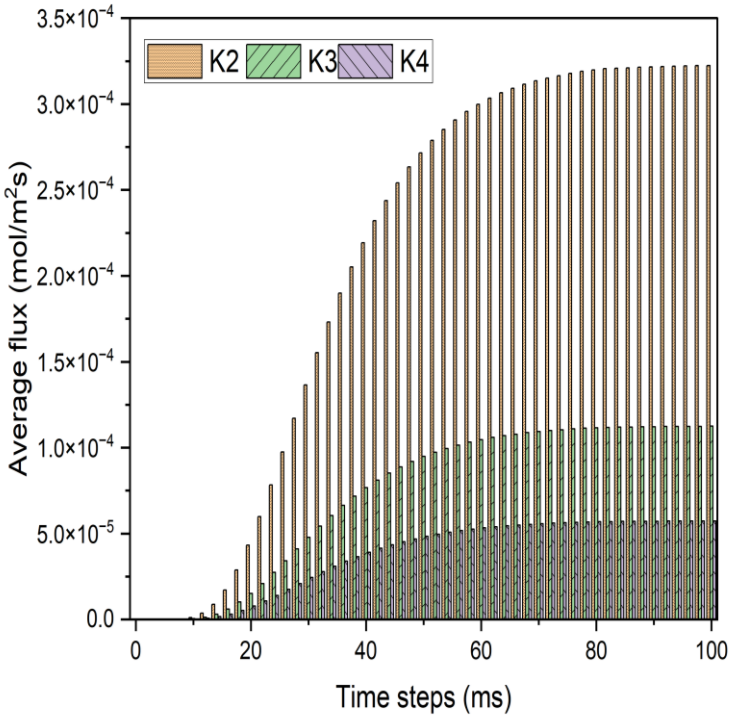

Figure 5. Difference in the average flux case for K2, k3 and K4 models compared to K1.

Flux difference plots relative to the K_1 model provide direct comparisons of K's impact. The flux difference $\Delta J\_Ki(t) = J\_Ki(t) - J\_K_1(t)$ starts at zero, peaks, then decays towards a small, non-zero steady-state value. Peak differences are substantial, with the K_4 model showing a maximum difference of nearly 0.005 mol/m²/s, almost doubling the flux compared to K_1. These differences underscore K's significant influence on species transport rates, particularly during early diffusion stages when concentration gradients are steepest.

3.3. Contour Plots of Concentration, Average Flux, and Total Flux Streamlines.

The transient concentration distributions and average flux results demonstrate the of the mass transfer coefficient K on transient diffusion reported the behavior significant impact in a transient concentration distributions and average flux results in a two-dimensional porous domain. Higher K values shows the increased concentration gradients which means the faster diffusion front propagation, and rapid boundary concentration depletion, compared to K_1 model.

Differences in concentration profiles are evaluated by surface plots which indeed provides a comprehensive analysis of spatiotemporal concentration. The average flux analysis predicts the K critical role in governing species transport behavior across boundaries. Higher K values result in higher peak fluxes. Flux differences relative to the K_1 model quantify these effects, emphasizing the importance of accurately modeling mass transfer boundary conditions in diffusion problems. Combining one-dimensional flux plots and relative difference plots offers a thorough quantitative analysis of K's impact on species transport rates in porous domains.

The contour plots of concentration, average flux, and total flux streamlines for the diffusion models with varying mass transfer coefficients (K_1 = 2.5 m/s, K_2 = 5 m/s, K_3 = 7.5 m/s, K_4 = 10 m/s) provide an in-depth visual analysis of the spatial and temporal of species transport over a 50 ms simulation period. These contours help to understand the local behavior of the diffusion process and also assists to predict the impact of the mass transfer boundary condition.

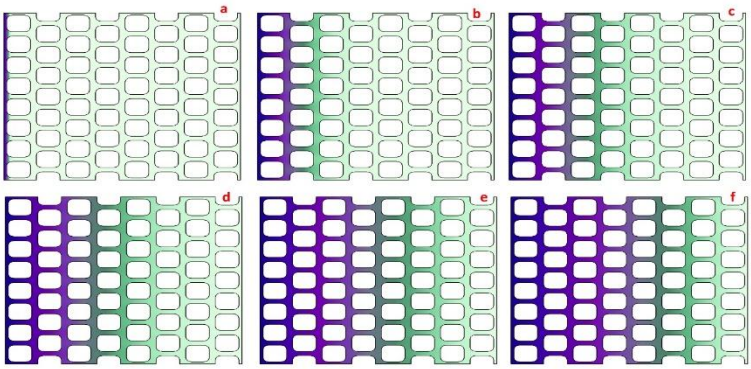

Figure 6. Surface concentration for the model at various timesteps of a) 0 ms b)2 ms c)6 ms d) 10 ms e)20 ms f)50 ms when K=2.5 m/s

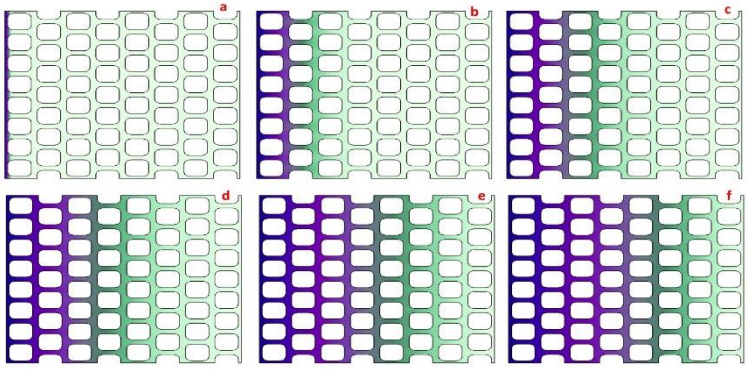

Figure 7. Surface concentration for the model at various timesteps of a) 0 ms b)2 ms c)6 ms d) 10 ms e)20 ms f)50 ms when K= 5 m/s

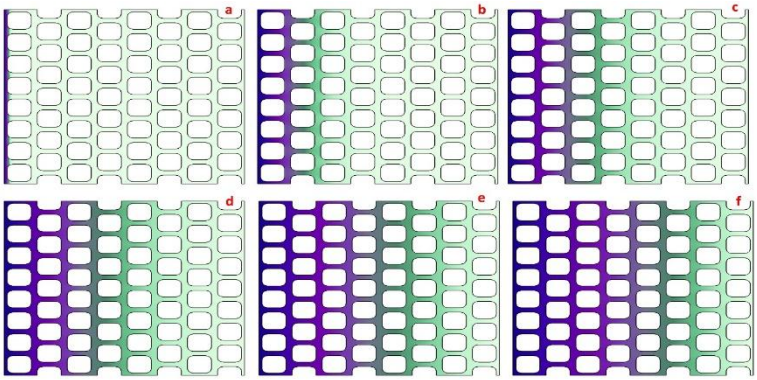

Figure 8. Surface concentration for the model at various timesteps of a) 0 ms b)2 ms c)6 ms d) 10 ms e)20 ms f)50 ms when K=7.5 m/s

The concentration plots illustrate in figure 6-8 the two-dimensional distribution of species concentration at various timesteps. At t = 0 ms, all models start with the identical initial profile, reporting the peak concentration of 3 mol/m³ near the left side of the boundary. As timestep size increases, the contours reveal the propagation of the diffusion front from left to right. The contour lines represent iso-concentration curves, with higher densities indicating steeper gradients. The effect of K on the concentration distribution is evident from the series of figures. The concentration front advances more progressively, maintaining a relatively high concentration near the left boundary for a longer duration for both K1 and K2. However, K3 and K4 result in sharper gradients and faster diffusion. The concentration front moves more rapidly towards the right boundary, and the overall concentration levels decrease more quickly.

The contour lines represent iso-flux curves, with higher densities indicating regions of higher flux. At t = 0 ms, the flux is zero everywhere, as the concentration gradient is initially zero. As the diffusion front propagates, the flux contours reveal the areas of highest species transport. The impact of K on the flux distribution is significant. Higher K values lead to higher flux magnitudes, as evident from the more intense colors. The flux is highest near the right boundary, where the mass transfer condition is applied. As K increases, the peak flux region

becomes more concentrated near the boundary and extends further into the right side of the domain. This is mainly due to the higher K enhances the rate of species removal at the boundary.

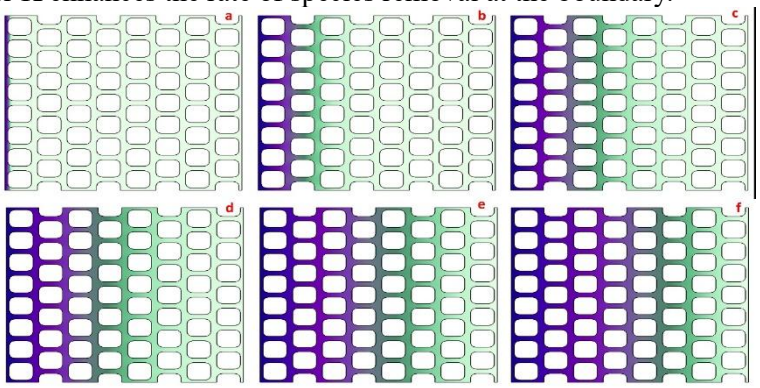

Figure 9. Surface concentration for the model at various timesteps of a) 0 ms b)2 ms c)6 ms d) 10 ms e)20 ms f)50 ms when K=10 m/s

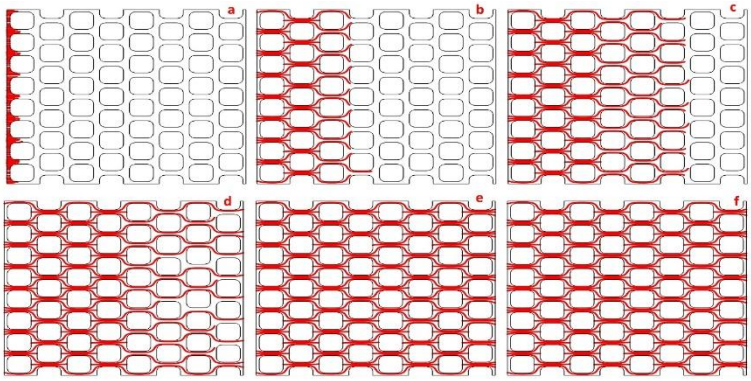

Figure 10. Total flux streamline model for various timesteps of a) 0 ms b)2 ms c)6 ms d) 10 ms e)20 ms f)50 ms when K=2.5 m/s

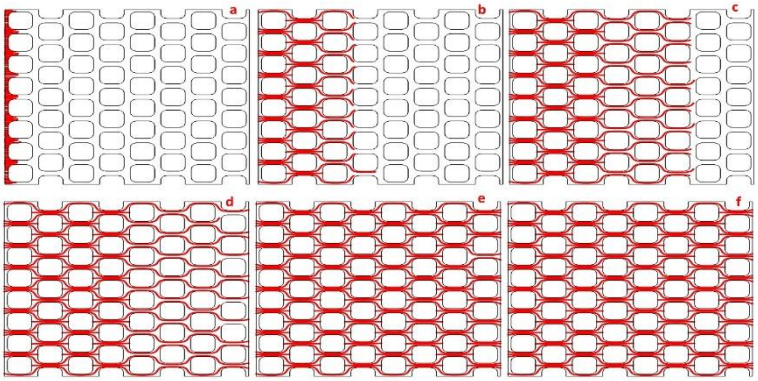

Figure 11. Total flux streamline model for various timesteps of a) 0 ms b)2 ms c)6 ms d) 10 ms e)20 ms f)50 ms when K=5 m/s

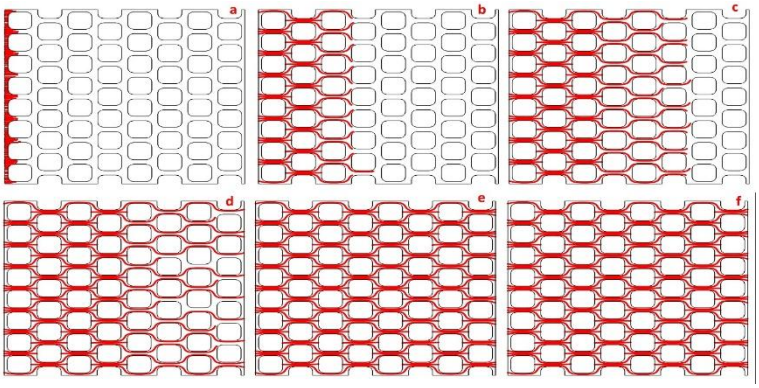

Figure 12. Total flux streamline model for various timesteps of a) 0 ms b)2 ms c)6 ms d) 10 ms e)20 ms f)50 ms when K=7.5 m/s

The total flux streamlines contours provide a directionality and magnitude of species transport effects on the K. The streamlines represent the paths along which species are transported indicating the relative flux magnitude. Figure 10-13 shows the total flux streamline model for various timesteps of 0 ms, 2 ms, 6 ms, 10 ms, 20 ms, 50 ms. when K=10 m/s at t = 0 ms, the streamlines tubes are uniform and parallel, reflecting the initial concentration gradient. As diffusion progresses, the streamlines bend and converge towards the right boundary, showing the direction of net species transport. The effect of K on the streamline patterns is notable. For K1 and K2 model, the streamlines are more evenly distributed and maintain a relatively uniform direction. This indicates a more gradual and balanced transport of species across the domain. However, the model K3 and K4, the streamlines become more concentrated and curved near the right boundary owing to the influence of the mass transfer conditions. In addition to that, strong flux towards the boundary were the other key reasons to consider. As the flux increases this leads to the acceleration in the removal of species. As the timestep size increases, the streamline patterns evolve differently for each K value. For lower K, the streamlines maintain a more uniform distribution, indicating a slower approach. For higher K, the streamlines rapidly concentrate near the right boundary and then become more evenly distributed.

4. Conclusion

The study provides detailed analysis of the effects of varying mass transfer coefficients on the transient diffusion and convection of a dilute chemical species 2D porous domain. The results demonstrate the significant impact of the mass transfer boundary condition on the spatiotemporal evolution of species concentration, average flux, and total flux streamlines.

- Higher mass transfer coefficients result in increased concentration gradients, faster diffusion front propagation, and rapid boundary concentration depletion. The concentration profiles illustrate that larger K values lead to sheer gradients and more uniform concentration distributions over time which help the system to reach faster equilibration.
- The average flux analysis reveals that higher K values yield higher peak fluxes and earlier occurrence of peak flux due to reduced boundary mass transfer resistance. The flux differences relative to the lowest K model quantify the substantial impact of K on species transport rates, particularly during early diffusion stages.
- The contour reveals the local behavior of the diffusion process and the influence of the mass transfer boundary condition. Higher K values result in more concentrated and curved streamlines near the right boundary, indicating accelerated species removal and transport towards the boundary.

In summary, accurately modeling the mass transfer boundary condition is crucial for correctly predicting species transport behavior in porous domains. The study highlights the need for careful consideration of mass transfer coefficients in diffusion-related applications and processes involving porous media. The current study helps the diffusion model is the catalytic reactor industry, particularly in the design and optimization of heterogeneous catalytic reactors involving porous catalysts.

5. References

1. Wang M, Gao B, Tang D. Review of key factors controlling engineered nanoparticle transport in porous media. Journal of hazardous materials. 2016 Nov 15;318:233-46.
2. Sen TK, Khilar KC. Review on subsurface colloids and colloid-associated contaminant transport in saturated porous media. Advances in colloid and interface science. 2006 Feb 28;119(2-3):71-96.
3. Simmons CT, Fenstemaker TR, Sharp Jr JM. Variable-density groundwater flow and solute transport in heterogeneous porous media: approaches, resolutions and future challenges. Journal of contaminant hydrology. 2001 Nov 1;52(1-4):245-75.
4. Thananukul K, Kaewsaneha C, Opaprakasit P, Lebaz N, Errachid A, Elaissari A. Smart gating porous particles as new carriers for drug delivery. Advanced Drug Delivery Reviews. 2021 Jul 1;174:425-46.
5. Tanimu A, Jaenicke S, Alhooshani K. Heterogeneous catalysis in continuous flow microreactors: A review of methods and applications. Chemical Engineering Journal. 2017 Nov 1;327:792-821.
6. Baqer Y, Chen X. A review on reactive transport model and porosity evolution in the porous media. Environmental Science and Pollution Research. 2022 Jul;29(32):47873-901.

7. Chen L, He A, Zhao J, Kang Q, Li ZY, Carmeliet J, Shikazono N, Tao WQ. Pore-scale modeling of complex transport phenomena in porous media. Progress in Energy and Combustion Science. 2022 Jan 1;88:100968.
8. Berre I, Doster F, Keilegavlen E. Flow in fractured porous media: A review of conceptual models and discretization approaches. Transport in Porous Media. 2019 Oct;130(1):215-36.
9. Taheri-Shakib J, Hosseini SA, Kazemzadeh E, Keshavarz V, Rajabi-Kochi M, Naderi H. Experimental and mathematical model evaluation of asphaltene fractionation based on adsorption in porous media: Dolomite reservoir rock. Fuel. 2019 Jun 1;245:570-85.
10. Fu J, Thomas HR, Li C. Tortuosity of porous media: Image analysis and physical simulation. Earth-Science Reviews. 2021 Jan 1;212:103439.
11. Chen L, He A, Zhao J, Kang Q, Li ZY, Carmeliet J, Shikazono N, Tao WQ. Pore-scale modeling of complex transport phenomena in porous media. Progress in Energy and Combustion Science. 2022 Jan 1;88:100968.
12. Haghi AK. Transport phenomena in porous media: A review. Theoretical Foundations of Chemical Engineering. 2006 Jan;40(1):14-26.
13. Lopez-Vizcaino R, Yustres A, Cabrera V, Navarro V. A worksheet-based tool to implement reactive transport models in COMSOL Multiphysics. Chemosphere. 2021 Mar 1;266:129176.
14. Baqer Y, Chen X. A review on reactive transport model and porosity evolution in the porous media. Environmental Science and Pollution Research. 2022 Jul;29(32):47873-901.
15. Jafari A, Vahab M, Broumand P, Khalili N. An eXtended finite element method implementation in COMSOL multiphysics: Thermo-hydro-mechanical modeling of fluid flow in discontinuous porous media. Computers and Geotechnics. 2023 Jul 1;159:105458.
16. Ullo J. Computational challenges in the search for and production of hydrocarbons. Scientific Modeling and Simulation SMNS. 2008 Apr;15(1):313-37.
17. Criddle CS, Alvarez LM, McCarty PL. Microbial processes in porous media. Transport processes in porous media. 1991:639-91.
18. Zare M, Hashemabadi SH. CFD simulation and experimental validation of tortuosity effects on pellet-fluid heat transfer of regularly stacked multi-lobe particles. Chemical Engineering Journal. 2019 Apr 1;361:1543-56.
19. Dentz M, Le Borgne T, Englert A, Bijeljic B. Mixing, spreading and reaction in heterogeneous media: A brief review. Journal of contaminant hydrology. 2011 Mar 1;120:1-7.
20. Khaled AR, Vafai K. The role of porous media in modeling flow and heat transfer in biological tissues. International Journal of Heat and Mass Transfer. 2003 Dec 1;46(26):4989-5003.
21. El-Zehairy AA, Nezhad MM, Joekar-Niasar V, Guymer I, Kourra N, Williams MA. Pore-network modelling of non-Darcy flow through heterogeneous porous media. Advances in Water Resources. 2019 Sep 1;131:103378